

Isotopic Dating of Strain Fringe Increments: Duration and Rates of Deformation in Shear Zones

Wolfgang Müller,^{1*} Domingo Aerden,² Alex N. Halliday¹

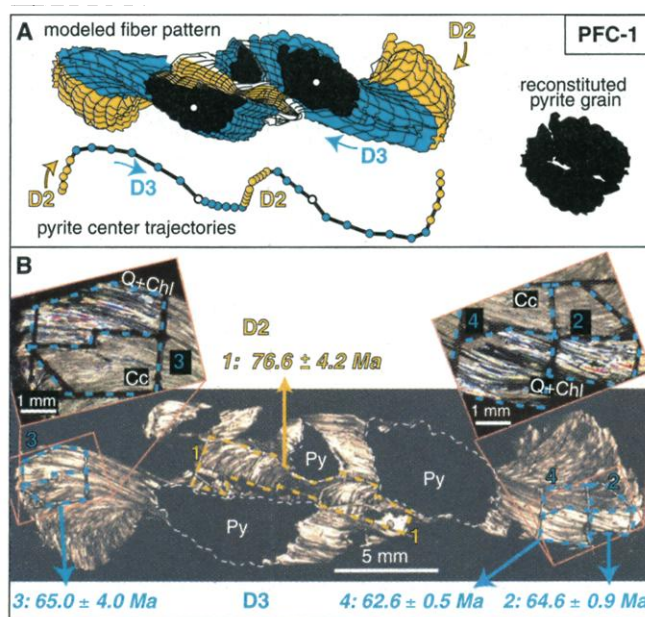
The time scales over which deformation in the Earth's crust remains localized in shear zones are poorly known, as are the associated strain rates. We have determined the longevity and rates of deformation using rubidium-strontium (Rb-Sr) microsampling dating of increments of fibrous strain fringes from a Pyrenean shear zone. The fibers grew quasi-continuously through a protracted deformation history between 87 and 50 million years ago, over a period comparable to that of an orogeny. During a short interval between 66 and 62 million years, a rise in strain rate from 1.1×10^{-15} to 7.7×10^{-15} seconds⁻¹ occurred. This acceleration correlates with an abrupt change in fiber-growth direction and a stress-field inversion from gravitational collapse to renewed horizontal crustal shortening.

It is unclear over what time scales deformation within the Earth's crust remains localized at distinct shear zones or faults. The rate at which crustal deformation progresses and its variation with time are also poorly constrained, yet are crucial for extrapolating experimental results to, and for modeling of, lithospheric processes. Natural strain rates are derived from geodetic surveys across active faults, or from sea-floor spreading, both yielding rates between 10^{-13} to 10^{-15} s⁻¹ (1). How such strain rates for the brittle upper crust relate to long-term processes in the ductile (lower) crust is unknown. Certain shear zones may be characterized by high strain rates [$>10^{-13}$ s⁻¹ (2)]. Our inability to link a sequence of deformations with a precise chronology has hampered the determination of these key parameters of lithospheric processes.

We have used syntectonic crystal fibers forming strain fringes around pyrite grains to link chronology and deformation by application of texturally controlled Rb-Sr microsampling dating (3) to increments of strain fringe growth. Strain fringes provide a kinematic record of how strain accumulated in a deforming rock (4), which can be related to the tectonic history of a region (5–7). Fibrous strain fringes up to ~12 mm long surrounding large (~5 mm) pyrites were collected from mylonitic carbonate-rich slates of Aptian age (~110 million years ago (Ma)) in the immediate hanging wall of a north-directed thrust of the Northern Pyrenees near Lourdes, France. The deforma-

tion and uplift of the Pyrenees recorded in these strain fringes resulted from the opening of the Bay of Biscay, the subsequent counterclockwise rotation of Iberia, and the final oblique collision with stable Europe along a major sinistral wrench system (North Pyrenean Fault) starting in the Early Cretaceous and finishing in the Late Oligocene (8–10). Associated high-temperature, low-pressure metamorphism dated between 105 and 85 Ma developed in a narrow belt bordering the North Pyrenean Fault (11), located ~10 km south of the sampling area. Since ~87 Ma, metamorphism became low-grade and deformation reached more external parts of the Pyrenees, i.e., the North and South Pyrenean Zones (11).

Fig. 1. Kinematic reconstruction (A) and photomicrographs (B) of PFC-1. (A) Modeled fiber pattern and resulting pyrite center trajectory (7, 15). The earlier deformation phase D2 is indicated in yellow, whereas subsequent deformation phase D3 is indicated in blue. Arrows indicate the direction of fiber growth. (B) Photomicrographs of the analyzed thick section and magnified images of the three D3 increments (crossed polarizers), with microdrilling cuts before extraction of the microsamples (yellow dashed lines indicate D2 and blue dashed lines indicate D3). Py, pyrite; Cc, calcite; Q+Chl, quartz+chlorite. The Rb-Sr microsampling ages that correspond to each analyzed increment are given below. The achievable spatial resolution of ~2 mm is controlled by the amount of chlorite-quartz fibers necessary for a sufficiently precise Rb-Sr age.



Microstructural analysis (7) of the strain fringes revealed two distinct phases of deformation called D2 and D3 (12) of the polyphase evolution (10) of the North Pyrenean Zone (north of North Pyrenean Fault). The D2 and D3 deformations postdate an earlier period of crustal shortening (D1), whose associated foliation forms straight inclusion trails in the pyrite grains. The pyrites therefore grew as post-D1 metamorphic crystals (porphyroblasts). The entire deformation sequence was interpreted (7) as having resulted from an episode of gravitational collapse (D2) between periods of crustal shortening (D1 and D3). Gravity-driven thrusting (D2) caused fringe growth and crenulation-cleavage development in the horizontal plane, whereas renewed horizontal shortening (D3) led to continued fringe growth and a second crenulation-cleavage in a steeply south-dipping plane. Extension directions around pyrite grains are not directly recorded by individual fibers, but can be reconstructed with the pyrite-center-trajectory (PCT) technique (7). PCTs consistently show a sharp bend recording the sudden change in fringe-growth direction between D2 and D3 (Figs. 1 to 4).

The strain fringes are composed of cogenetic calcite, quartz, and chlorite, representing a lower greenschist facies mineral assemblage (Figs. 1 and 2). The fringes form <10- to 100- μ m thin fibers that typically are several millimeters long. Fringe growth was antitaxial, i.e., from the matrix interface directed toward the pyrite, and displacement-controlled, i.e., fibers track particle paths. The textural relations between the intergrown and mineralogically different fibers and the absence of recrystallization or alteration are

¹Institut für Isotopengeologie und Mineralische Rohstoffe, Department Erdwissenschaften, Sonneggstrasse 5, ETH Zürich, CH-8092 Zürich, Switzerland.

²Departamento de Geodinámica, Universidad de Granada, E-18071 Granada, Spain.

*To whom correspondence should be addressed. E-mail: wolfgang.mueller@erdw.ethz.ch

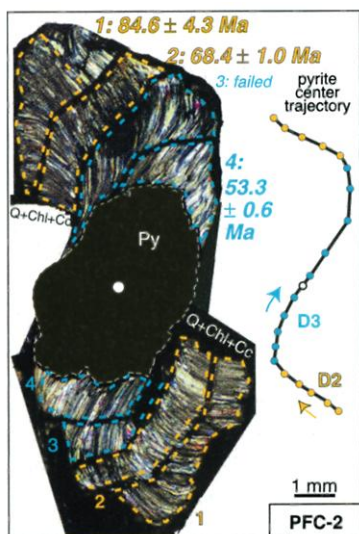


Fig. 2. Photomicrograph of PFC-2 with cut microsamples composed of strongly intergrown chlorite, quartz, and calcite fibers spanning their entire evolution (dashed lines with the same color coding as in Fig. 1). The microsamples had a spatial resolution of ~1 mm due to the combination of corresponding increments from both sides of the pyrite. The pyrite center trajectory shows the characteristic hook shape indicating the change from D2 to D3 deformation (7, 15). The resulting Rb-Sr ages are given next to the corresponding increment.

consistent with contemporaneous growth. Chlorite + quartz should have high Rb/Sr ratios compared with co-genetic calcite (13), making them suitable for Rb-Sr dating. On the basis of microstructures and available zircon fission-track ages (14), the temperature of deformation (D2 + D3) is constrained to be <300°C, so the Rb-Sr ages date mineral growth (13). It is possible to precisely analyze $\leq 10^{-9}$ g of Sr (3), the amount present in $< 5 \times 10^{-4}$ g for the investigated minerals with low Rb-Sr concentrations. Such samples are small enough to be extracted from rock thick sections (~40 to 50 μ m), allowing full textural control.

Two large pyrite-fringe complexes (PFCs) from the same hand specimen cut parallel to the lineation and perpendicular to the foliation were studied. A large (35-mm-long) pyrite-fringe complex, referred to as PFC-1, consists of three pieces of an originally round pyrite (diameter ~9 mm) that was torn apart during deformation, forming a complex fiber pattern (Fig. 1). The growth of the fibers was reconstructed by a series of translation-rotation operations as detailed in (7). The resulting pyrite center trajectory revealed the relative pyrite-matrix movement and guided sampling of age-equivalent fibers from thick section along fiber-isogrowth lines (Fig. 1A). Fibers belonging to the initial phase of deformation D2 occur both at the distal ends as well as in between the pyrites, where calcite-quartz-chlorite fibers spanning the whole evolution of D2 have been microsampled (increment 1, Fig. 1B). The following

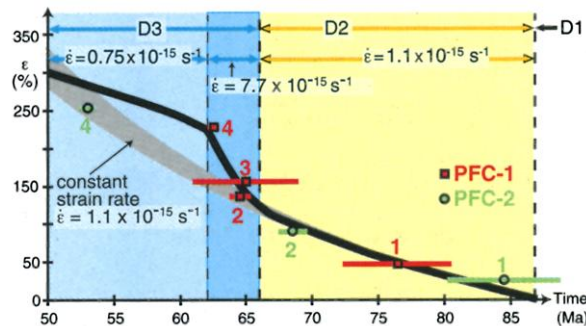


Fig. 3. Graph plotting the dated strains. Curves of constant strain rate (for both PFCs) define the gray area. The solid black line connecting data points is our model strain rate that exhibits the accelerated strain rate (dark blue) between D2 (yellow) and D3 (blue) deformation.

phase of deformation D3 was sampled in two successive increments on one side (increments 2 and 4) and another increment on the opposite side (increment 3), in position approximately corresponding to increment 2 (Fig. 1B). Calcite and quartz + chlorite could be physically separated in case of all four increments (3). Increment 1, the only sample corresponding to the initial deformation phase D2, yields a Rb-Sr age of 76.6 ± 4.2 Ma (Table 1 and Fig. 1B). Increments 2 and 4, representing two successive increments of the next deformation phase D3, define younger ages of 64.6 ± 0.9 and 62.6 ± 0.5 Ma, respectively. Increment 3 gives an age of 65.0 ± 4.0 Ma, similar to the opposite but corresponding position at increment 2. These four ages are consistent with the antiaxial growth direction of the fringes. The earliest and latest fiber increments could not be dated from PFC-1 because they contained only calcite.

To constrain the whole growth interval, we analyzed a second pyrite-fringe complex (PFC-2). PFC-2 is a simpler strain fringe with one central pyrite of diameter ~4 mm and characteristically hooked fibers on both sides that are

each ~4-mm long (Fig. 2). Fibers were microsampled following the reconstructed fiber-isogrowth-lines, which yielded four successive increments of about similar length on each side. The corresponding increments from both sides were put together to form one larger sample and to derive more precise ages. Increments 1 and 2 belong to the initial deformation phase D2, whereas increments 3 and 4 represent different stages of the subsequent phase D3. The most distal increment 1 (furthest away from the pyrite) yields an age of 84.6 ± 4.3 Ma and is followed by increment 2 dated at 68.4 ± 1.0 Ma (Table 1 and Fig. 2). Increment 3 gives an anomalously old age of 177 ± 2 Ma. Reexamination of the photographs taken before extraction of increment 3 revealed previously unseen traces of mica-rich matrix material in between the newly formed fibers, which may have been passively dragged into the growing fibers along the fuzzy margin of increment 3 (Fig. 2, arrow). A first-order calculation of such an admixture indicates that ~0.5 to 1% modal abundance of old (Variscan), Sr-rich mica would be sufficient to offset the low-Sr chlorite/quartz fibers to the final result. This is consistent with the

Table 1. Rb-Sr microsampling isotopic data (qc, quartz + chlorite; cc, calcite) (3). Quoted errors of $^{87}\text{Sr}/^{86}\text{Sr}$ ratios include errors of measurement and blank correction, which was based on total procedure blanks of 6.9 ± 0.7 pg (1 σ ; Rb) and 13.6 ± 1.9 pg ($^{87}\text{Sr}/^{86}\text{Sr} = 0.7108 \pm 9$; 1 σ ; $n = 3$; Sr), respectively. The error of the $^{87}\text{Rb}/^{86}\text{Sr}$ ratio is 0.25% (1 σ) for silicates and 2.5% (1 σ) for carbonates. Errors refer to the least significant digits of the corresponding values. Ages are calculated for the qc - cc pair of each increment; the age given in brackets is interpreted to be geologically meaningless.

Sample number	Sample weight (μ g)	Rb (ppm)	Sr (ppm)	$^{87}\text{Rb}/^{86}\text{Sr}$	$^{87}\text{Sr}/^{86}\text{Sr}$ ($\pm 95\%$ c.l.)	Age (Ma)
PFC-1 cc1	1971.3	0.016	1366	0.00014	0.708719 ± 9	
PFC-1 qc1	603.4	1.62	4.796	0.9798	0.709785 ± 58	76.58 ± 4.24
PFC-1 cc2	327.9	0.306	1476	0.00060	0.708721 ± 8	
PFC-1 qc2	525.7	3.50	2.123	4.780	0.713104 ± 55	64.55 ± 0.88
PFC-1 cc3	717.0	0.045	1508	0.00009	0.708751 ± 8	
PFC-1 qc3	892.5	0.762	1.048	2.106	0.710696 ± 118	65.00 ± 3.97
PFC-1 cc4	391.3	0.215	1392	0.00045	0.708804 ± 13	
PFC-1 qc4	794.2	7.81	3.711	6.100	0.714231 ± 30	62.63 ± 0.49
PFC-2 cc1	845.5	0.038	1168	0.00009	0.708706 ± 10	
PFC-2 qc1	348.2	1.89	7.536	0.7195	0.709571 ± 42	84.62 ± 4.25
PFC-2 cc2	531.5	0.203	1041	0.00056	0.708693 ± 9	
PFC-2 qc2	744.1	4.92	5.336	2.670	0.711285 ± 35	68.35 ± 1.01
PFC-2 cc3	137.3	0.072	911.8	0.00023	0.708917 ± 10	
PFC-2 qc3	778.3	1.968	2.336	2.442	0.715061 ± 61	[177.0 ± 2.0]
PFC-2 cc4	213.8	0.283	1060	0.00077	0.708935 ± 14	
PFC-2 qc4	641.4	18.14	13.46	3.904	0.711891 ± 24	53.31 ± 0.57

REPORTS

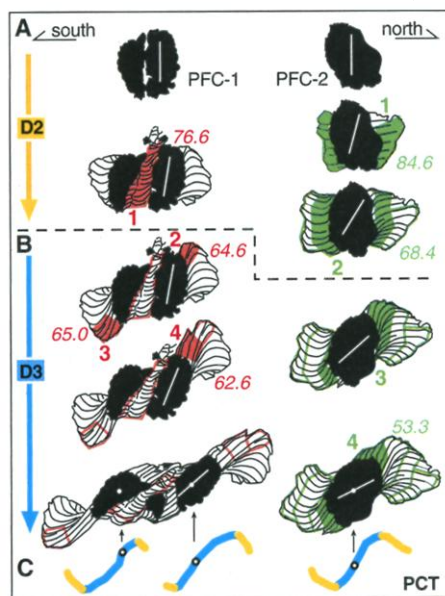


Fig. 4. Evolution of PFC-1 and PFC-2 with growth increments corresponding to dated microsamples (large red and green numbers) of deformation phase D2 (A) and D3 (B) (7, 15). Corresponding ages are given in italics. Color-coding of hook-shaped pyrite-center trajectories (PCT) (C) indicates D2 and D3 fringe portions (Fig. 1). The fibers themselves curve more smoothly than the PCTs, because of body rotations of pyrites (white marker lines) and fringes, additional to translations.

amount of matrix material observed. The most proximal increment 4 yields an age of 53.3 ± 0.6 Ma. The higher Rb-Sr concentrations of increment 4 are likely due to the minute amounts of newly grown white mica fibers observed. The ages of the three increments 1, 2, and 4 of PFC-2 are consistent with the growth direction inferred from microstructural analysis.

The accuracy of the presented two-point Rb-Sr microsampling ages relies on isotopic equilibration among the phases analyzed. In the present case, all minerals are newly

grown fibers with equilibrium textures. Because the analyzed increments yielded a sequence of ages consistent with the direction of fiber growth (with the exception of increment 3 from PFC-2, see above) and reproducible ages are obtained for corresponding positions (compare increments 2 and 3 of PFC-1), the ages are considered to reliably date the growth of the fibers.

Integrating the results of the two samples permits determining the timing of transition of the regional stress field between deformation phases D2 and D3. This shift from gravitational collapse to renewed horizontal compression is bracketed by increment 2 of PFC-2 (D2: 68.4 ± 1.0 Ma) and increment 2 of PFC-1 (D3: 64.6 ± 0.9 Ma) to have occurred at 66 ± 1 Ma. A strain versus time diagram (Fig. 3 and Table 2) was calculated as in (15) and was used to assess the temporal evolution of the strain fringes. The finite strain recorded by PFC-2 and PFC-1 is 280 and 330%, respectively. In order to compute strain rates, we determined the whole period of fiber growth by extrapolating the results of the most distal and proximal increments 1 and 4 of PFC-2. Their midpoints record ages of 84.6 ± 4.3 and 53.3 ± 0.6 Ma, respectively, for which fiber growth was extrapolated to have started at 87 Ma and ended at 50 Ma. Hence, the investigated strain fringes record quasi-continuous deformation over an interval of ~ 37 million years (My), which is consistent with the onset of deformation within the Pyrenees at ~ 90 to 85 Ma (8–11) and the final uplift of the North Pyrenean Zone at 48 to 32 Ma, as constrained by apatite fission-track ages (14). Our data imply that the shear zone was active over the entire period of deformation in the foreland. Hence, single deformation ages (16) may become questionable, as time intervals reflect the evolution of shear zones better.

The calculated progressive strain curves for both samples (15) yielded an average

strain rate of $1.1 \times 10^{-15} \text{ s}^{-1}$ (Fig. 3), showing how strain and time would have been related at constant strain rate. However, if the data for the D3 increments of PFC-1 are plotted into the strain-time diagram, an acceleration of deformation for the period between ~ 66 and ~ 62 Ma is indicated. During this interval of ~ 4 My, the strain rate rose by more than half an order of magnitude to $7.7 \times 10^{-15} \text{ s}^{-1}$. This increase in strain rate correlates well with the onset of renewed horizontal compression during D3 deformation, which is interpreted to have acted as the cause for more rapid deformation in the foreland. Between 62 and 50 Ma, deformation decelerates again, and the strain rate drops to $0.75 \times 10^{-15} \text{ s}^{-1}$.

The calculated strain rates are below $1 \times 10^{-14} \text{ s}^{-1}$ and therefore close to the lower boundary estimated for natural strain rates of deformed rocks (1). However, two effects contribute to these low strain rates. First, the sample investigated was not collected from the center of the regional shear zone but comes from its immediate hanging wall, because it is where the strain fringes occur. This sample therefore records lower finite strain than the shear zone itself, although higher strain than most other rocks in the area. Second, the D3 strain of the pyrite-fringe complexes provides only a lower limit for D3 strain in the sample, because the long axes of the complexes were aligned subhorizontally at the start of D3, and only progressively rotated toward the long axes of the D3 strain ellipse (15). The same does not apply to D2 strain, because it started with an equidimensional pyrite. Hence, the obtained strain rates are considered to be minimum values.

The microsamples are too large to distinguish whether fibers grew continuously or in a (discontinuous) crack-seal manner (17). If the latter were true, then averaging over the whole time span would yield an underestimation of the effective rate of fiber growth. However, this does not affect strain rates in the surrounding rock, because crack-seal fiber growth is a cyclic response of veins or strain fringes to continuous deformation around them. The long period of fiber growth points to the possibility of protracted strain localization at comparatively low rates within the upper crust during tens of millions of years, comparable with the duration of an orogeny.

References and Notes

1. O. A. Pfiffner and J. G. Ramsay, *J. Geophys. Res.* **87**, B1, 311 (1982).
2. S. M. Schmid, *Ecolae Geol. Helv.* **68**, 247 (1975).
3. W. Müller, N. Mancktelow, M. Meier, *Earth Planet. Sci. Lett.*, in press. Only a brief summary is given, emphasizing the modifications necessary because of the peculiar sample mineralogy. After cutting the fiber increments with a microscope-mounted microdrill, subsequent cleaning, and weighing, the quartz + chlorite microsamples were leached twice to ensure

Table 2. Incremental strain data of both dated PFCs (15).

Microsample increment	Incremental strain	Cumulative strain	Age (Ma)	Dated strain
		<i>PFC-1</i>		
Start D2	0.00	0.00	87.0 extrapolated	0.00
Increment 1	1.03	1.03	76.58 ± 4.24	0.47
End D2	0.00	1.03	66.0 interpolated	1.03
Increment 2	0.34	1.72	64.55 ± 0.88	1.36
Increment 3	0.55	2.15	65.00 ± 3.97	1.56
Increment 4	0.42	2.88	62.63 ± 0.49	2.28
End D3	0.37	3.30	50.0 extrapolated	3.30
		<i>PFC-2</i>		
Start D2	0.00	0.00	87.0 extrapolated	0.00
Increment 1	0.55	0.55	84.62 ± 4.25	0.26
Increment 2	0.46	1.28	68.35 ± 1.01	0.90
End D2	0.00	1.28	66.0 interpolated	1.28
Increment 3	0.44	2.27	Failed	1.75
Increment 4	0.16	2.81	53.31 ± 0.57	2.54
End D3	0.00	2.81	50.0 extrapolated	2.81

- separation of silicates from residual carbonates with 500 μl of $\sim 8\text{ M}$ acetic acid in an ultrasonic bath ($\sim 10\text{ min}$) and on a warm hotplate ($\sim 15\text{ min}$) with a 500- μl rinse of water in between. Subsequently, the sample was leached with warm 2.5 M HCl for $\sim 5\text{ min}$, followed by another rinse with 500 μl of water. All leachates and rinses were collected and analyzed; they contained $\leq 6\%$ of Sr that previously resided in the silicates. After addition of a ^{84}Sr - ^{85}Rb tracer, the silicate samples were dissolved in closed fluorinated ethylene propylene (FEP) vials at $\sim 80^\circ\text{C}$ with 400 μl of concentrated HF and 10 μl of concentrated HNO_3 (3 days) and equilibrated with 400 μl of 6M HCl overnight. The solutions were scrutinized with a binocular microscope and found to be free of undissolved particles or precipitates. Carbonate samples were dissolved with 500 μl of $\sim 8\text{ M}$ acetic acid. All sample weights of PFC-2 and the silicate sample weights of PFC-1 are given according to the estimated modal abundances deduced from thick section. Measured values for the SRM987 Sr standard were 0.710292 ± 13 (1σ ; static mode Faraday; 10 to 100 ng of Sr; $n = 23$).
4. J. G. Ramsay and M. I. Huber, *The Techniques of Modern Structural Geology*, vol. 1, *Strain Analysis* (Academic Press, London, 1983).
 5. D. Dietrich, *Tectonophysics* **170**, 183 (1989).
 6. D. Fischer and T. Byrne, *Tectonics*, **11**, 330 (1992).
 7. D. G. A. M. Aerden, *J. Struct. Geol.* **18**, 75 (1996).
 8. J.-L. Olivet, *Bull. Cent. Rech. Explor. Prod. Elf Aquitaine* **20**, 131 (1996).
 9. W. R. Roest and S. P. Srivastava, *Geology* **19**, 613 (1991).
 10. P. Choukroune, *Annu. Rev. Earth Planet. Sci.* **20**, 143 (1992).
 11. J.-M. Goldberg and H. Maluski, *C. R. Acad. Sci. Ser. II* **306**, 429 (1988).
 12. A deformation phase is defined as a time interval with a constantly oriented stress field. The distinction of D1, D2, and D3 deformation phases at Lourdes is based on field investigations and microstructural analysis revealing a superposition of three tectonic foliations (S1, S2, and S3), as well as geometric modeling of PFCs yielding hook-shaped pyrite-center trajectories parallel to S2 and S3 (7).
 13. W. Müller, R. D. Dallmeyer, F. Neubauer, M. Thöni, *J. Geol. Soc. London* **156**, 261 (1999).
 14. L. J. Garwin, thesis, Cambridge University (1985).
 15. On the basis of kinematic reconstruction (Fig. 4), D2 strains were measured by the change in length (Δl) of a line (l_0) connecting the external terminations of opposite fringes (strain = $\Delta l/l_0$). D3 strains were calculated by treating the pre-D3 PFC as three rigid fragments being pulled apart (as normal boudinage),

whereby the gap between fragments is filled by D3 fibers. D3 strain corresponds to the length change of a line connecting the midpoints of the original D2 fringes. Microsamples were cut according to the shape of successive D2 and D3 growth increments. They represent time intervals, so their ages correspond to about their median line, although the older half represents slightly more strain than the younger half (l_0 differs for both). This difference was taken into account for calculation of the dated strains (Table 2). Quantitative errors in this procedure are negligible because length changes can be measured very precisely. Qualitative errors in the (manual) kinematic reconstruction are considered small as seen from the close match between true and modeled fibers (Figs. 1 and 2).

16. S. R. Freeman, S. Inger, R. W. H. Butler, R. A. Cliff, *Tectonics* **16**, 57 (1997).
17. J. G. Ramsay, *Nature* **284**, 135 (1980).
18. We thank N. Mancktelow for discussions, T. Willi for thick-section preparation, and M. Meier for lab support. Reviews by two anonymous reviewers and comments by D. Dietrich, J. G. Ramsay, and A. B. Thompson helped to improve the manuscript and are gratefully acknowledged.

19 January 2000; accepted 11 April 2000

Coherent High- and Low-Latitude Climate Variability During the Holocene Warm Period

Peter deMenocal,^{1*} Joseph Ortiz,¹ Tom Guilderson,² Michael Sarnthein³

A faunal record of sea-surface temperature (SST) variations off West Africa documents a series of abrupt, millennial-scale cooling events, which punctuated the Holocene warm period. These events evidently resulted from increased southward advection of cooler temperate or subpolar waters to this subtropical location or from enhanced regional upwelling. The most recent of these events was the Little Ice Age, which occurred between 1300 to 1850 A.D., when subtropical SSTs were reduced by 3° to 4°C . These events were synchronous with Holocene changes in subpolar North Atlantic SSTs, documenting a strong, in-phase link between millennial-scale variations in high- and low-latitude climate during the Holocene.

The warm climate of the Holocene epoch [the last 11,700 thousand years (11.7 ky B.P.)] conventionally has been viewed as climatically stable (1) with little evidence of the abrupt millennial-scale climatic shifts that characterize glacial periods (2, 3). Oxygen isotopic records from central Greenland ice cores indicate essentially no Holocene variability, with the notable exception of the Preboreal and early Holocene cooling events

near 10 and 8.2 thousand years ago (ka) (4). However, recently developed Holocene paleoclimate records from ice cores and high-latitude marine sediments show that Holocene climate was also unstable, having been punctuated by several significant, millennial-scale cooling events, which recurred roughly every 1500 ± 500 years (5–8). The most recent of these Holocene cooling events was the Little Ice Age between ca. 1300 to 1870 A.D. (5, 9), when Scandinavian glaciers attained their furthest expansion since 9 ka (10).

Unlike for high latitudes, little is known about the possibility of such millennial-scale climate variability in lower latitudes. Furthermore, the mechanisms underlying this variability remain unclear. Understanding this

mode of climate variability is particularly relevant because it represents a natural, recurrent climatic instability, which evidently operates independently of the size of high-latitude ice sheets as these ~ 1500 -year cooling events occurred during both glacial and interglacial climatic extrema (7). Here we investigate the timing, amplitude, and nature of low-latitude climate variability during the Holocene, and demonstrate that high- and low-latitude climates were coupled by quantifying past SST variations preserved in a well-dated, high-accumulation-rate sediment core off West Africa.

Ocean Drilling Program Hole 658C was cored off Cap Blanc, Mauritania ($20^\circ 45'\text{N}$, $18^\circ 35'\text{W}$; 2263 m water depth) (11) during the Ocean Drilling Program (ODP) Leg 108 (Fig. 1). Sediment accumulation rates are high at this site (22 cm/ky average) due, in part, to the dual influences of high regional surface ocean productivity and high supply of windblown African mineral dust. Strong seasonal upwelling and high productivity results from the strong northeast trade winds, which parallel the Northwest African margin (12). Hole 658C is also positioned within the axis of the summer African eolian dust plume (Fig. 1), which transports Saharan mineral aerosol dust to the adjacent subtropical Atlantic Ocean (13). The site is well situated to monitor past changes in regional ocean circulation because it lies within an oceanographic boundary separating cooler temperate and subpolar waters to the north from warmer tropical water masses to the south and west (Fig. 1).

Core 1H from Hole 658C was continuously subsampled at 2-cm intervals, which is equivalent to between 50 and 100 years temporal resolution. Samples were analyzed for calcium carbonate and biogenic opal percent-

¹Lamont-Doherty Earth Observatory of Columbia University, Palisades, NY 10964, USA. ²Center for Accelerator Mass Spectrometry, Lawrence-Livermore National Laboratory, Livermore, CA 94551, USA. ³Institut für Geowissenschaften, Universität Kiel, Kiel, Germany.

*To whom correspondence should be addressed. E-mail: peter@ldeo.columbia.edu